INFLUENCE OF SINTERING TEMPERATURE ON STRUCTURE AND OPTICAL PROPERTIES OF $BiFeO_3$-$BaTiO_3$ MATERIALS

Nguyen Ngoc Minh[1], Vu Trong Truong[1], Bui Van Dan[1], Pham Ngoc Thang[1], Nguyen Thi Thu[2], Pham Van Tuan[3], Ngo Duc Quan[4*]

[1]Hung Yen University of Technology and Education, [2]University of Economics - Technology for Industries, [3]School of Materials Science and Engineering - Hanoi University of Science and Technology
[4]Hanoi University of Science and Technology

ARTICLE INFO

Received: 07/3/2025
Revised: 09/5/2025
Published: 09/5/2025

KEYWORDS

BFO-BTO
Multiferroic
Optical properties
Lead-free materials
Sol-gel

ABSTRACT

The multiferroic $0.7BiFeO_3$-$0.3BaTiO_3$ materials was synthesized via the sol-gel method at sintering temperatures of 800 ºC, 850 ºC, 900 ºC, and 950 ºC to examine the effect of sintering temperature on its structure and optical properties. X-ray diffraction analysis confirmed the coexistence of the rhombohedral R3c phase of $BiFeO_3$ and the tetragonal P4mm phase of $BaTiO_3$. With increasing sintering temperature, a gradual transition from the rhombohedral phase to the tetragonal phase was observed. Furthermore, the grain size of the material increased as the sintering temperature rose. The optical bandgap (E_g) of $BiFeO_3$- $BaTiO_3$ decreased slightly from 2.02 eV at 800 ºC to 1.96 eV at 950 ºC. These structural and optical changes are attributed to the phase transition from rhombohedral to tetragonal symmetry induced by higher sintering temperatures. This study highlights the influence of sintering temperature on the structure and optical properties of $BiFeO_3$- $BaTiO_3$, demonstrating its potential for multifunctional devices when sintered at optimal temperatures.

ẢNH HƯỞNG CỦA NHIỆT ĐỘ KẾT TINH LÊN CẤU TRÚC VÀ TÍNH CHẤT QUANG CỦA VẬT LIỆU $BiFeO_3$-$BaTiO_3$

Nguyễn Ngọc Minh[1], Vũ Trọng Trường[1], Bùi Văn Dân[1], Phạm Ngọc Thắng[1], Nguyễn Thị Thu[2], Phạm Văn Tuấn[3], Ngô Đức Quân[4*]

[1]Trường Đại học Sư phạm Kỹ thuật Hưng Yên, [2]Trường Đại học Kinh tế Kỹ thuật Công nghiệp
[3]Trường Vật liệu - Đại học Bách khoa Hà Nội, [4]Đại học Bách khoa Hà Nội

THÔNG TIN BÀI BÁO

Ngày nhận bài: 07/3/2025
Ngày hoàn thiện: 09/5/2025
Ngày đăng: 09/5/2025

TỪ KHÓA

BFO-BTO
Đa pha
Tính chất quang
Vật liệu không chì
Sol-gel

TÓM TẮT

Vật liệu $0,7BiFeO_3$-$0,3BaTiO_3$ được tổng hợp thông qua phương pháp sol-gel ở các nhiệt độ kết tinh là 800 ºC, 850 ºC, 900 ºC và 950 ºC nhằm khảo sát ảnh hưởng của nhiệt độ nung đến cấu trúc và tính chất quang của vật liệu. Phân tích nhiễu xạ tia X cho thấy sự tồn tại đồng thời của pha mặt thoi R3c của $BiFeO_3$ và pha tứ giác P4mm của $BaTiO_3$. Khi nhiệt độ nung tăng lên, một sự chuyển pha từ pha mặt thoi sang pha tứ giác đã xảy ra. Hơn nữa, kích thước hạt tinh thể của vật liệu tăng lên khi nhiệt độ nung tăng. Năng lượng vùng cấm (E_g) của $BiFeO_3$- $BaTiO_3$ giảm nhẹ từ 2,02 eV ở 800 ºC xuống còn 1,96 eV ở 950 ºC. Những thay đổi về cấu trúc và tính chất quang này là do quá trình chuyển pha từ kiểu đối xứng mặt thoi sang pha tứ giác khi nhiệt độ nung cao gây ra. Nghiên cứu này nhấn mạnh ảnh hưởng của nhiệt độ nung đến cấu trúc và tính chất quang của $BiFeO_3$- $BaTiO_3$, cho thấy tiềm năng ứng dụng của vật liệu cho các thiết bị đa chức năng khi nhiệt độ kết tinh được tối ưu.

DOI: https://doi.org/10.34238/tnu-jst.12235

[*] Corresponding author. *Email: quan.ngoduc@hust.edu.vn*

1. Introduction

Multiferroic materials have garnered significant research interest in recent years due to their unique coexistence of ferroelectric and magnetic properties [1]. These materials hold immense potential to revolutionize various technological fields, including electromagnetic wave attenuation, solar cells, multi-state memory devices, photocatalysis, and spintronics [2] – [6]. While lead-based materials such as $Pb(Zr,Ti)O_3$ (PZT) have been foundational in information and electronic technologies, their toxicity and environmental impact have been widely documented [5], [7]. This has driven the pursuit of sustainable lead-free alternatives, with notable progress achieved using $BiFeO_3$ (BFO), a non-toxic multiferroic material that exhibits both G-type antiferromagnetic order (Néel temperature, T_N ~ 643 K) and ferroelectric order (Curie temperature, T_C ~ 1100 K) [8], [9]. The ferroelectric properties of BFO are primarily attributed to the lone pair electrons in the 6s orbital of Bi^{3+}, while its magnetic properties arise from the electronic occupancy of the d orbitals in Fe [7], [10]. BFO's remarkable magnetoelectric coupling and high remnant polarization make it a compelling subject of research [11]. However, its antiferromagnetic order is characterized by weak magnetism due to the spatial modulation of its spin structure, influenced by antiferromagnetic superlattices [12]. Additionally, BFO's high oxygen vacancy density and significant leakage current, resulting from bismuth evaporation and the variable valence of iron (Fe^{2+} to Fe^{3+}), compromise its ferroelectric performance [13]. Furthermore, changes in the Fe-O-Fe bond angle and the distribution of FeO_6 octahedra can reduce saturation magnetization [14], [15]. Structural inhomogeneities and oxygen vacancies can also significantly alter BFO's electromagnetic properties [16], potentially limiting its practical applications. To address these challenges, strategies such as reducing crystal grain size, cation substitution, and combining BFO with other perovskites have been explored [14] – [16]. Among these, the combination of $BiFeO_3$ with $BaTiO_3$ (BTO) has shown promising results in enhancing ferromagnetic, ferroelectric, and electromagnetic properties. BFO-BTO ceramics have emerged as strong candidates to replace PZT, as BFO and BTO exhibit rhombohedral (R) and tetragonal (T) structures, respectively, at room temperature (RT), with high phase transition temperatures (T_C ~ 825 °C) [17] – [19]. Venevtsev et al. [20] proposed that BF-BT forms a continuous solid solution at RT with three crystal structures: R (100-67% BF), C (67-7.5% BF), and T (7.5-0% BF), a finding later confirmed by Kumar et al. [21]. Leontsevw and Eitel [22] presented a phase diagram for the BF-BT system based on temperature-dependent permittivity (ε_r) and differential scanning calorimetry (DSC) measurements, identifying a wide temperature-independent morphotropic phase boundary (MPB) between the R and C phases (0.25-0.4 BT), which enhances piezoelectric properties. Lee et al. [23] further reported an R-T-like MPB in rapidly cooled BF-BT ceramics, achieving a d_{33} of 402 pC/N and a T_C of 454 °C.

A clear resemblance exists between PZT and BF-BT, with both systems exhibiting a phase migration trend from R to T as the concentrations of BT and PT increase. However, a key distinction lies in the site occupancy: in BF-BT, both A and B sites are occupied by multiple ion types, whereas PZT involves only the B site. This difference influences the phase composition transitions between the two systems. In BF-BT, Ba acts as a larger blocking ion, inhibiting the displacement of isolated Bi, while at the B site, the competition between Fe and Ti induces a displacement. This competitive shift across both sites drives the formation of pseudo-symmetrical structures with short-range order, as observed by Leontsevw and Eitel [22].

In this study, the multiferroic material $0.7BiFeO_3$-$0.3BaTiO_3$ (BFO-BTO) was synthesized using the sol-gel method at sintering temperatures of 800 ºC, 850 ºC, 900 ºC, and 950 ºC. The research aims to investigate the effect of sintering temperature on the material's structure and optical properties, observe changes in structural phase content and surface morphology as a function of sintering temperature, and analyze variations in the optical bandgap (E_g) of BFO-BTO. The study elucidates the influence of sintering temperature on the structural and optical properties of BFO-BTO, demonstrating its potential for multifunctional devices when sintered at optimal temperatures.

2. Experimental Details

The $0.7BiFeO_3$-$0.3BaTiO_3$ (BFO-BTO) nanomaterials were synthesized using the sol-gel method. The raw materials consisted of bismuth nitrate pentahydrate ($Bi(NO_3)_3.5H_2O$, TQ, 98%), iron nitrate nonahydrate ($Fe(NO_3)_3.9H_2O$, TQ, 99.9%), barium acetate ($(CH_3COO)_2Ba$, TQ, 99.9%), and titanium (IV) isopropoxide ($C_{12}H_{28}O_4Ti$, TQ, 98%). Acetic acid (CH_3COOH) and acetylacetone ($CH_3COCH_2COCH_3$) were used as solvents in a 1:1 volume ratio. In the first step, $Bi(NO_3)_3.5H_2O$, $Fe(NO_3)_3.9H_2O$, and $(CH_3COO)_2Ba$ were dissolved in acetic acid and distilled water to form a transparent solution. In the second step, acetylacetone was added to the solution, followed by the introduction of titanium (IV) isopropoxide. The mixture was stirred for approximately 6 hours at room temperature to obtain a transparent sol. In the third step, the sol was heated at 100 °C to produce a dry gel. In the final step, the dried gel was crushed and calcined at 400 °C for 2 hours, followed by sintering at temperatures of 800 °C, 850 °C, 900 °C, and 950 °C for 5 hours. To evaluate the morphology of the samples, scanning electron microscopy (SEM) was employed. The crystal structure was characterized using X-ray diffraction (XRD), while the optical properties were investigated through UV-Vis absorption spectroscopy.

Table 1. *Structural parameters of BFO-BTO materials obtained by the Rietveld method*

Sanples	800 ºC		850 ºC		900 ºC		950 ºC	
	R3c	**P4mm**	**R3c**	**P4mm**	**R3c**	**P4mm**	**R3c**	**P4mm**
Lattice parameter (Å)	5.4759	4.0015	5.4803	4.0023	5.4807	4.0022	5.4840	4.0022
	15.0025	3.9999	15.0008	4.0005	14.9920	4.0007	14.9891	4.0010
Proportion (%)	65.82	34.18	65.01	34.99	61.22	38.78	64.13	35.87
Goodness of Fit (G.o.f)	1.4		2.0		1.6		1.8	
χ^2	1.53		2.94		2.62		2.90	
Rexp	25.6		24.2		17.9		20.7	
D (nm)	42.1		42.7		54.5		57.3	

3. Results and Discussion

The kinetics of the reactions leading to the formation of BFO-BTO oxides were examined using thermogravimetric (TG) and derivative thermogravimetric (DTG) analyses, as illustrated in Figure 1. The formation of BFO-BTO, with nitrates serving as precursors and acetic acid, distilled water, and acetylacetone as solvents, can be broken down into several stages: (1) the removal of hydrate groups, (2) the formation of hydroxides, (3) the decomposition of hydroxides into metal carbonates, and finally (4) the nucleation of BFO-BTO phases. The TG analysis reveals an overall weight loss of approximately 49.3%. At 200 °C, there is a significant weight reduction of nearly 25% due to the release of water vapor, hydrate ions, and nitrogen compounds. Between 200 and 275 °C, the weight loss of about 19.5% is associated with the breakdown of metal hydroxides. A smaller weight loss of approximately 2.2% occurs in the range of 275 to 500 °C, likely due to the evaporation of different carbonates. In the temperature interval of 500 to 800 °C, the sample experiences minimal weight change, remaining around 0.35%. However, above 800 °C, the weight loss begins to increase, reaching about 1.2% at 950 °C, indicating significant vaporization of Bi^{3+} ions at temperatures above 800 °C. The DTG curve shows two discernible exothermic peaks at around 100 °C and 240 °C, likely corresponding to the decomposition of bismuth hydroxide and iron hydroxide, respectively. After 300 °C, the nucleation of BFO-BTO starts, influenced by secondary phases that emerge due to varying energy requirements for the decomposition of precursor hydroxides. The Differential Thermal Analysis (DTA) curve displays three identifiable peaks at approximately 496 °C, 710 °C, and 800 °C, linked to the crystallization of several intermediate phases as well as the main BFO-BTO phase. Importantly, a slight weight loss of about 0.35% was noted between 500 and 800 °C, which is likely attributed to the growth

of BFO-BTO crystals and the elimination of surface-adsorbed materials. The outcomes from DTA, TG, and DTG analyses contributed to identifying the optimal thermal processing and synthesis temperatures for the materials under investigation.

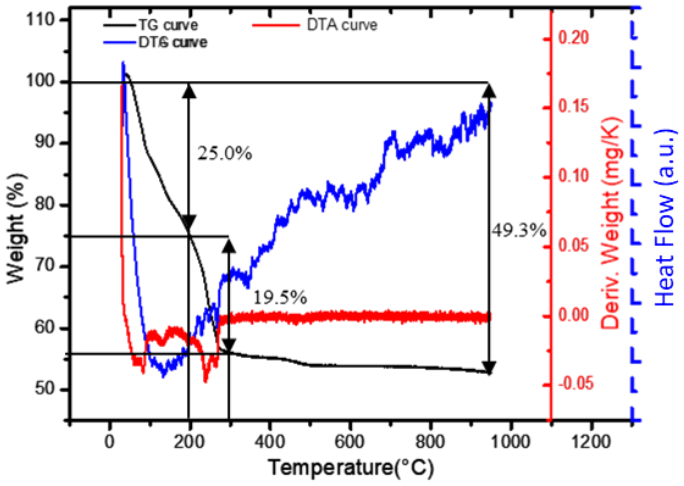

Figure 1. *TG, DTA, and DTG curves of BFO-BTO samples*

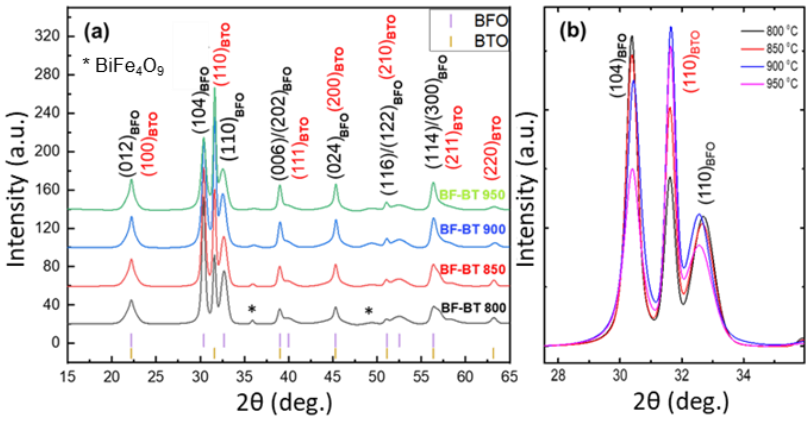

Figure 2. *(a) XRD pattern of BFO-BTO samples and (b) XRD pattern in the range of 2θ from 28° to 35°*

Figure 2 shows the XRD patterns of BFO-BTO samples sintered at different temperatures. The results reveal that, alongside peaks corresponding to the main perovskite phase of BFO-BTO, the sample sintered at 700 °C displays several diffraction peaks associated with the intermediate phase $BiFe_4O_9$ (marked with an asterisk) around 2θ ~ 36° and 50° [24]. The intensity of these unusual peaks is relatively strong, highlighting a significant presence of $BiFe_4O_9$. The formation of intermediate phases in the BFO sample may result from: (i) impurities in the precursors, and (ii) the dominance of thermodynamic reaction kinetics ($\Delta G > 0$), where ΔG represents the Gibbs free energy of the equilibrium reaction between BFO and secondary phases [25]. It is well known that temperature and holding times during crystallization play critical roles in controlling chemical reaction kinetics. As the sintering temperature increases, the distinct diffraction peaks of the intermediate phases diminish significantly. For samples sintered at 900 °C, the contribution from impurity intermediate phase diffraction signals is minimal, indicating that 900 °C is the optimal crystallization temperature for BFO-BTO materials.

XRD patterns reveal the coexistence of two structural phases in BFO-BTO samples. The rhombohedral structure of BFO, belonging to the R3c group, shows distinct peaks corresponding to JCPDS card no. 86-1518. The double peaks (104)/(110) and (006)/(202) are clearly observed

around diffraction angles of 2θ ~ 32° and 39.5°, respectively. Simultaneously, the XRD pattern also displays peaks characteristic of the tetragonal P4mm phase of BTO, corresponding to JCPDS card no. 05-0626 [26]. The well-separated double peaks at 2θ = 30.4° and 32.7° are attributed to the (104) and (110) planes of the BFO rhombohedral phase, along with the (110) peak at 31.6° from the BTO tetragonal phase. The sharp and well-defined peaks indicate that the BFO-BTO samples have well-crystallized structures. As the sintering temperature increases, the XRD patterns show a noticeable shift in the intensity of the double peaks. The intensity of the (104) and (110) peaks for BFO gradually decreases, while the intensity of the (110) peak at 31.6° for BTO increases significantly. This suggests a phase transition from the distorted rhombohedral structure to the tetragonal structure. The phase transition from the distorted rhombohedral type to tetragonal or orthorhombic configurations, or into two-component phases, depends primarily on the fabrication method, sintering temperature and time, the type of substituting ions, and their concentration [27].

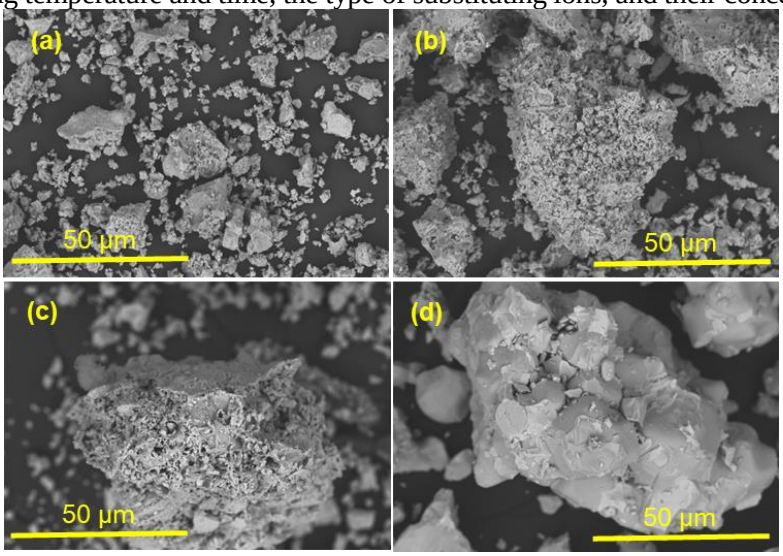

Figure 3. *SEM images of BFO-BTO samples at at different sintering temperatures: (a) 800 °C, (b) 850 °C, (c) 900 °C, and (d) 950 °C*

To further investigate the structural phase transition of BFO-BTO with respect to sintering temperature, XRD analysis based on the Rietveld method was conducted using MAUD software. The crystal lattice parameters are presented in Table 1. From Table 1, it is evident that the lattice parameters of BFO and BTO in the material samples undergo slight changes. However, the phase composition ratio of BFO/BTO within the material shows significant variations. The content of the rhombohedral phase of BFO decreases from 65.82% for the sample sintered at 800 °C to 61.22% for the sample sintered at 900 °C, while the percentage of the tetragonal phase of BTO increases from 34.18% for the sample sintered at 800 °C to 38.78% for the sample sintered at 900 °C.

Furthermore, the Scherrer equation is utilized to calculate the average crystalline sizes of BFO-BTO using the (104)/(110) preferred orientations from the XRD data. The formula is represented as:

$$D = \frac{K\lambda}{\beta cos(\theta)} \quad (1)$$

In this context, the constants D, K, λ, β, and θ denote the grain size, Scherrer constant (with a theoretical value of K being 0.89), wavelength (0.15406 nm), Full Width at Half Maximum (FWHM), and Bragg angle, respectively. Table 1 shows that the D value significantly rises from 42.1 nm to 57.3 nm as the sintering temperature increases. This finding aligns perfectly with the results observed in the SEM images presented in Figure 3.

Figure 3 presents the SEM images of BFO-BTO materials as a function of sintering temperature. The images reveal that the morphology of BFO-BTO particles evolves with increasing sintering temperature. At lower sintering temperatures, the particles exhibit flake-like

morphologies with smaller grain sizes. The material appears porous, marked by numerous voids and poorly defined grain boundaries. As the sintering temperature increases, the particle structure becomes denser, with more compact and well-defined grain boundaries. To explore changes in the optical bandgap (E_g), the energy band structure of the samples was analyzed using UV-Vis absorption spectroscopy, with the results depicted in Figure 4. The data show strong absorption peaks for the BFO-BTO samples within the wavelength range of 250 nm to 580 nm, corresponding to electronic transitions associated with Fe-O [28]. This suggests that the synthesized BFO-BTO samples exhibit strong interactions with visible light. The optical bandgap E_g values for the samples were calculated using the Tauc equation: $\alpha h\gamma = A(h\gamma - E_g)^n$. Based on prior research, BFO-BTO is characterized by a direct band transition, with n equal to ½ [29].

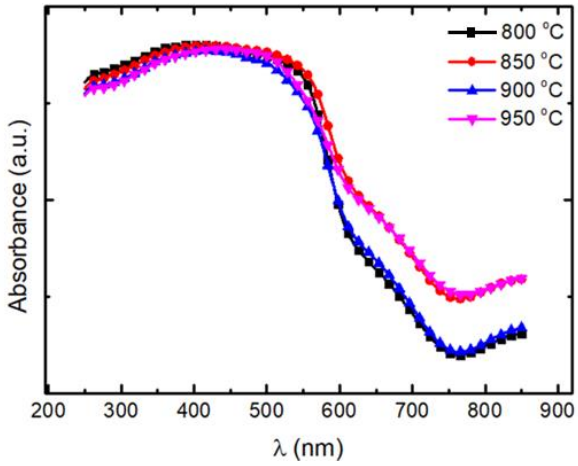

Figure 4. *Ultraviolet-visible (UV-Vis) absorption spectra of BFO-BTO samples*

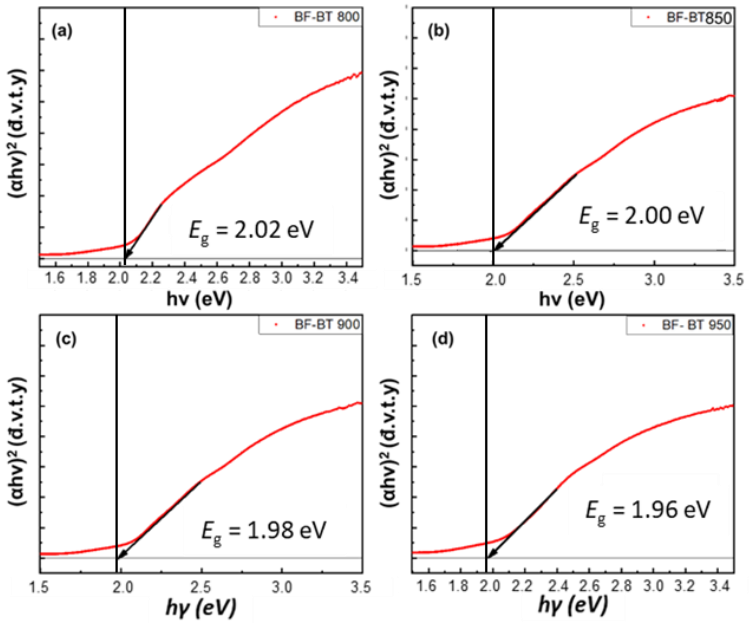

Figure 5. *Tauc plots of $(\alpha h\nu)^2$ versus the photon energy ($h\nu$) for BFO-BTO samples crystallized at: (a) 800 ℃, (b) 850 ℃, (c) 900 ℃, and (d) 950 ℃*

Figures 5 depicts the relationship between $(\alpha h\gamma)^2$ and $h\gamma$ for the BFO-BTO samples. The linear segments of these curves, when extrapolated to the x-axis, enable the determination of the optical bandgap. Figure 5.a shows that the bandgap of the BFO-BTO sample crystallized at 800

ºC is 2.02 eV. This value is consistent with the study by Catalan and colleagues, which reports that the bandgap energy of BFO is 2.1 eV [17]. However, this value differs significantly from the bandgap energy of BTO, which is approximately 3.0 eV, according to the publication by Ren and co-authors [26]. This indicates that the BFO phase plays a crucial role in the optical properties of the material. The calculated bandgap energies for the BFO-BTO samples exhibit a consistent decline as the sintering temperature increases, dropping from 2.02 eV at 800 ºC to 1.96 eV at 950 ºC. This reduction in bandgap energy is associated with lattice distortion and the reconfiguration of molecular orbitals in the octahedral FeO_6 structure, driven by the increased presence of the BTO phase. These changes modify the microstrain within the BFO-BTO structure, enhancing its light absorption spectrum in the visible range. Additionally, this phenomenon may be explained by the Burstein-Moss effect, where lower energy states in the conduction band are occupied by electrons, inhibiting further electronic transitions to the bottom of the conduction band in the presence of defects [30]. Our findings suggest that BFO-BTO has significant potential for use in optoelectronic devices and infrared detectors.

4. Conclusion

The multiferroic $0.7BiFeO_3$-$0.3BaTiO_3$ (BFO-BTO) material was successfully synthesized via the sol-gel method while varying sintering temperatures from 800 ºC to 950 ºC. XRD analysis revealed a transition in the structural composition of BFO-BTO from the rhombohedral R3c phase to the tetragonal P4mm phase with increasing sintering temperature. The content of the rhombohedral phase gradually transitioned to the tetragonal phase as the sintering temperature increased, alongside a corresponding increase in the material's grain size. The E_g value of BFO-BTO decreased from 2.02 eV for samples sintered at 800 ºC to 1.96 eV for those sintered at 950 ºC, reflecting the changes in optical properties with sintering temperature. This transformation is explained by the material's structural transition from rhombohedral R3c symmetry to tetragonal P4mm symmetry with higher sintering temperatures. This study has illuminated the impact of sintering temperature on the structure and optical properties of BFO-BTO. The results indicate that the multiferroic BFO-BTO material with optimal sintering temperature has potential applications in multifunctional devices.

Acknowledgements

This work is financially supported by the Ministry of Education and Training, Vietnam, under project number B2023–SKH-01.

REFERENCES

[1] D. D. Dang, Q. H. Nguyen, H. T. Nguyen, D. Q. Ngo, T. L. Le, H. L. Nguyen, H. T. Nguyen, N. T. Nguyen, and H. B. Luong, "Biferroic properties of Fe-doped Ba(Ti,Zr)O_3 materials," *Materials Letters*, vol. 283, 2021, Art. no. 128897.

[2] D. D. Dang, H. L. Nguyen, T. K. P. Le, H. T. Nguyen, H. B. Luong, T. T. Dang, V. V. Pham, D. Q. Ngo, and Q. V. Dang, "Optical properties of a new $(1-x)Bi_{1/2}Na_{1/2}TiO_3 + xPr_{1/2}Na_{1/2}TiO_3$ solid solution system," *Materials Letters*, vol. 302, 2021, Art. no. 130381.

[3] D. D. Dang, H. T. Nguyen, T. T. T. Chu, Q. H. Nguyen, H. B. Luong, H. T. Nguyen, D. Q. Ngo, N. T. Nguyen, and H. L. Nguyen, "Observation of the ferromagnetic and nonlinear dielectric properties of Mn-doped $0.8BaTiO_3$–$0.2BaZrO_3$ compounds," *Applied Physics A*, vol. 127, 2021, Art. no. 61.

[4] D. C. Nguyen, D. P. Bui, V.K. Phan, Q. D. Tran, T. A. Ho, T. H. Nguyen, V. C. Le, H. T. Nguyen, .T. M. H. Nguyen, D. D. Dang, D. Q. Ngo, M. D. Tran, T. L. Phan, D. T. Pham, and D. T. Bui, "Synthesis and Microwave Absorption Properties of Novel $Bi_{1/2}(Na_{0.8}K_{0.2})_{1/2}TiO_3/Fe_3O_4$ Composite," *Materials Transactions*, vol. 64, pp. 2450-2456, 2023.

[5] Q. D. Nguyen, H. L. Nguyen, X. D. Luong, V. V. Pham, D. Q Ngo, and D. D. Dang, "Enhanced room temperature ferromagnetism in $YMnO_3$-modified lead-free ferroelectric $Bi_{0.5}Na_{0.5}TiO_3$ materials," *Applied Physics A*, vol. 129, 2023, Art. no. 547.

[6] T. T. H. Le, T. T. Vu, D. Q. Ngo, X. T. Cao, T. T. Duong, D. H. Nguyen, N. K. Tran, and V. T. Pham, "Microstructure and photocatalytic activity of SnO_2:Bi^{3+} nanoparticles," *Optical Materials*, vol. 137, 2023, Art. no. 113552.

[7] D. Q. Ngo, V. T. Pham, D. M. Nguyen, and R. Guus, "Influence of heterostructure on structure, electric and magnetic properties of $Bi_{0.5}(Na_{0.80},K_{0.20})_{0.5}TiO_3/BaZrO_3$ films prepared by the sol–gel method," *Japanese Journal of Applied Physics*, vol. 62, 2023, Art. no. 040901.

[8] X. L. Liang, and J. Q. Dai, "Prominent ferroelectric properties in Mn-doped $BiFeO_3$ spin-coated thin films," *Journal of Alloys and Compounds*, vol. 886, 2021, Art. no. 161168.

[9] N. A. Spaldin and M. Fiebig, "The Renaissance of Magnetoelectric Multiferroics," *Science,* vol. 309, pp. 391-392, 2005.

[10] D. Q. Ngo, D. M. Nguyen, and R. Guus, "Influence of $BiFeO_3$ perovskite on the structure and magnetic properties of lead-free $Bi_{0.5}Na_{0.4}K_{0.1}TiO_3$ films," *Japanese Journal of Applied Physics*, vol. 60, 2020, Art. no. 010902.

[11] K. Fujii, H. Kato, K. Omoto, Ma. Yashima, J. Chen, and X. Xing, "Experimental visualization of the Bi–O covalency in ferroelectric bismuth ferrite ($BiFeO_3$) by synchrotron X-ray powder diffraction analysis," *Physical Chemistry Chemical Physics*, vol. 15, pp. 6779-6782, 2013.

[12] Y. Wang, and C. W. Nan, "Effect of Tb doping on electric and magnetic behavior of $BiFeO_3$ thin films," *Journal of Applied Physics*, vol. 103, 2008, Art. no. 024103.

[13] A. R. Makhdoom, M. J. Akhtar, M. A. Rafiq, and M. M. Hassan, "Investigation of transport behavior in Ba doped $BiFeO_3$," *Ceramics International*, vol. 38, pp. 3829-3834, 2012.

[14] D. Kothari *et al.*, "Study of the effect of Mn doping on the $BiFeO_3$ system," *Journal of Physics: Condensed Matter*, vol. 19, 2007, Art. no. 136202.

[15] W. Prellier, M. P. Singh, and P. Murugavel, "The single-phase multiferroic oxides: from bulk to thin film," *Journal of Physics: Condensed Matter*, vol. 17, 2005, Art. no. R803.

[16] C. Ederer, and N. A. Spaldin, "Influence of strain and oxygen vacancies on the magnetoelectric properties of multiferroic bismuth ferrite," *Physical Review B*, vol. 71, 2005, Art. no. 224103.

[17] G. Catalan and J. Scott, "Physics and Applications of Bismuth Ferrite," *Advanced Materials*, vol. 21, pp. 2463-2485, 2009.

[18] T. Rojac, A. Bencan, B. Malic, G. Tutuncu, J. Jones, J. Daniels, and D. Damjanovic, "$BiFeO_3$ Ceramics: Processing, Electrical, and Electromechanical Properties," *Journal of the American Ceramic Society*, vol. 97, 2014, Art. no. 12982.

[19] D. Wang, M. Wang, L. Fengbin, Y. Cui, Q. Zhao, H. Sun, H. Jin, and M. Cao, "Sol–gel synthesis of Nd-doped $BiFeO_3$ multiferroic and its characterization," *Ceramics International*, vol. 41, 2015, Art. no. 8768.

[20] I. H. Ismailzade, R. M. Ismailov, A. I. Alekberov, and F. M. Salaev, "Investigation of the magnetoelectric (ME) effect in solid solutions of the systems $BiFeO_3$-$BaTiO_3$ and $BiFeO_3$-$PbTiO_3$," *Physica Status Solidi (a)*, vol. 68, pp. K81-K85, 1981.

[21] M. M. Kumar, A. Srinivas, and S. Suryanarayana, "Structure Property Relations in $BiFeO_3/BaTiO_3$ Solid Solutions," *Journal of Applied Physics*, vol. 87, pp. 855-862, 2000.

[22] S. Leontsev, and R. Eitel, "Dielectric and Piezoelectric Properties in Mn-Modified $(1-x)BiFeO_3$–$xBaTiO_3$ Ceramics," *Journal of the American Ceramic Society*, vol. 92, pp. 2957-2961, 2009.

[23] M. H. Lee *et al.*, "High-Performance Lead-Free Piezoceramics with High Curie Temperatures," *Adv. Mater*, vol. 27, pp. 6976-6982, 2015.

[24] J. Zhao, S. Liu, W. Zhang, Z. Liu, and Z. Liu, " Structural and magnetic properties of Er-doped $BiFeO_3$ nanoparticles," *J. Nanopart. Res.*, vol. 15, 2013, Art. no. 1969.

[25] S. M. Selbach, M. A. Einarsrud, and T. Grande, "On the thermodynamic stability of $BiFeO_3$," *Chem. Mater*, vol. 21, 2009, Art. no. 169.

[26] P. Ren, H. Fan, and X. Wang, "Electrospun nanofibers of $ZnO/BaTiO_3$ heterostructures with enhanced photocatalytic activity," *Catalysis Communications*, vol. 25, pp. 32-35, 2012.

[27] A. Jindal, A. Agarwal, and P. Aghamkar, "Structural changes and magnetism in $Bi_{1-x}Ba_xFeO_3$ (x = 0, 0.1, 0.2, 0.3) nanopowders," *Applied Physics A*, vol. 124, 2018, Art. no. 323.

[28] B. Ramachandran, A. Dixit, R. Naik, G. Lawes, and M. S. R. Rao, "Charge transfer and electronic transitions in polycrystalline $BiFeO_3$," *Physical Review B*, vol. 82, 2010, Art. no. 012102.

[29] S. T. Zhang, Y. Zhang, M. H. Lu, C. L. Du, Y. F. Chen, Z. G. Liu, Y. Y. Zhu, N. B. Ming, and X. Q. Pan, "Substitution-induced phase transition and enhanced multiferroic properties of $Bi_{1-x}La_xFeO_3$ ceramics," *Applied Physics Letters*, vol. 88, 2006, Art. no. 162901.

[30] W. Zhou, H. Deng, H. Cao, J. He, J. Liu, P. Yang, and J. Chu, "Effects of Sm and Mn co-doping on structural, optical and magnetic properties of $BiFeO_3$ films prepared by a sol–gel technique," *Materials Letters*, vol. 144, pp. 93-96, 2015.